Mon. Not. R. Astron. Soc. **000**, 1–?? (2013) Printed 4 February 2014 (MN LATEX style file v2.2)

The Complex Distribution of Recently Formed Stars. Bimodal Stellar Clustering in the Star-Forming Region NGC 346.

Dimitrios A. Gouliermis,⋆ Sacha Hony, and Ralf S. Klessen
Universität Heidelberg, Zentrum für Astronomie, Institut für Theoretische Astrophysik, Albert-Ueberle-Str. 2, 69120 Heidelberg, Germany

arXiv:1402.0078v1 [astro-ph.GA] 1 Feb 2014

To be submitted to MNRAS

ABSTRACT

We present a detailed stellar clustering analysis with the application of the two-point correlation function on distinct young stellar ensembles. Our aim is to understand how stellar systems are assembled at the earliest stages of their formation. Our object of interest is the star-forming region NGC 346 in the Small Magellanic Cloud. It is a young stellar system well-revealed from its natal environment, comprising complete samples of pre–main-sequence and upper main-sequence stars, very close to their formation. We apply a comprehensive characterization of the autocorrelation function for both centrally condensed stellar clusters and self-similar stellar distributions through numerical simulations of stellar ensembles. We interpret the observed autocorrelation function of NGC 346 on the basis of these simulations. We find that it can be best explained as the combination of two distinct stellar clustering designs, a centrally concentrated, dominant at the central part of the star-forming region, and an extended self-similar distribution of stars across the complete observed field. The cluster component, similar to non-truncated young star clusters, is determined to have a core radius of ~ 2.5 pc and a density profile index of ~ 2.3. The extended fractal component is found with our simulations to have a fractal dimension of ~ 2.3, identical to that found for the interstellar medium, in agreement to hierarchy induced by turbulence. This suggests that the stellar clustering at a time very near to birth behaves in a complex manner. It is the combined result of the star formation process regulated by turbulence and the early dynamical evolution induced by the gravitational potential of condensed stellar clusters.

Key words: Magellanic Clouds – stars: pre-main-sequence – stars: statistics – HII Regions – ISM: individual objects: LHA 115-N66 – open clusters and associations: individual: NGC 346.

1 INTRODUCTION

It is generally accepted that stars form in groups of various sizes and characteristics (Lada & Lada 2003), starting with small compact concentrations of protostars embedded in star-forming regions and moving up in *length-scale* to large extended loose aggregates of young stars stars. It is, however, suggested that these diverse stellar assembles are not independent from each other, but tightly connected through the star formation process (Elmegreen 2011). Small, dense proto-clusters coexist in a symbiotic fashion with larger, less dense subgroups of OB-type stars, which in turn reside in even larger, looser stellar associations, each of these types of objects representing a different *time-scale* of star formation within one molecular cloud (Efremov & Elmegreen 1998). This picture of clustered star formation at various length- and time-scales is not always clear in our observations, as e.g., in the massive star formation environments of star-burst clusters.

Studies of newly formed stellar systems can identify the conditions that may favor *multiple* over *single* cluster formation events. Different scenarios for star formation predict different observable properties for the resulting stellar systems. The 'quiescent' star formation scenario (e.g. Krumholz & Tan 2007) predicts large age-spreads among young stars in the same molecular cloud, while according to the 'competitive accretion' scenario (e.g. Clark et al. 2007) star formation is a process of short time-scale, leading to clusters in a variety of forms.

The investigation of the clustering of stars at the time of their formation can provide important information on the nature of the star formation process itself (e.g., Schmeja et al. 2008), and place constraints to the suggested theories. A single compact stellar cluster, embedded in its own HII region, would suggest a local monolithic episode of star formation in a dense environment. However, such clusters are rarely found in isolation; they are the densest stellar concentrations of larger stellar structures as seen in dwarf and spiral galaxies (Efremov 2009; Karampelas et al. 2009). In our own Galaxy multiple (or fractured) clusterings of stars

⋆ dgoulier@mpia.de; dgoulierm@googlemail.com

in large star-forming regions, are also more commonly observed (Feigelson et al. 2011; Megeath et al. 2012). This clustering behavior favors the existence of multiple processes, such as feedback, controlling star formation, and being active on different scales.

Giant Molecular Clouds are hierarchical structures (Elmegreen & Falgarone 1996; Stutzki et al. 1998), indicating that scale-free processes determine their global morphology. Turbulence is being widely accepted as the dominant among these processes (Mac Low & Klessen 2004; Elmegreen & Scalo 2004). The goal of this paper is to establish whether the newly formed stars follow a similar, hierarchical distribution, which may indicate that turbulence also determines the clustering behavior of stars at the time of their formation. This investigation requires a complete census of stars, covering a high dynamic range in masses, distributed over the typical length-scale of giant molecular clouds.

Our target of interest is the star-forming complex NGC 346, the brightest H II region in the Small Magellanic Cloud (LHA 115-N66; Henize 1956). *Hubble* Space Telescope imaging of such regions in the Magellanic Clouds (MCs) provides an unprecedented access to their newly-born stellar populations down to the sub-solar regime over large areas of the sky. Observed by *Hubble* (GO Program 10248; PI: A. Nota), this region satisfies, thus, the main observational criteria for our analysis: 1) Observed on size-scales relevant for molecular clouds (50 - 100 pc); 2) High angular resolution ($\sim 0.125''$); 3) Large number of detected members, covering a significant fraction of the stellar Initial Mass Function, complete to ~ 0.5 M$_\odot$. Our dataset, obtained with the Advanced Camera for Surveys (ACS), is described in Gouliermis et al. (2006).

A rich sample of more than 98,000 stars was detected down to $m_{555} \simeq 27$ mag with $\gtrsim 50\%$ completeness. It comprises a mixture of stellar generations, with 60% of the stars formed $\lesssim 5$ Gyr ago (Cignoni et al. 2011). The young populations in NGC 346 consist mainly of low-mass pre–main-sequence (PMS) stars, identified from their positions on the color-magnitude diagram (see Gouliermis 2012, for a review on low-mass PMS stars in the Magellanic Clouds). It is decidedly troublesome to determine an age for a cluster based on its PMS stars (Jeffries 2012; Preibisch 2012). Nevertheless, an isochronal age of ~ 3 Myr has been established for NGC 346 by Sabbi et al. (2008) by comparison with PMS evolutionary models. We complete the sample of low-mass PMS stars with the upper–main-sequence (UMS) stars ($m_{555} - m_{814} \leqslant 0.0$ mag; $12 \lesssim m_{555} \lesssim 17$ mag; ages $\lesssim 10$ Myr), compiling a total sample of 5,150 stars. The UMS stars correspond to about 7% of the sample. The map of our stellar inventory is shown in Figure 1.

In a previous study (Schmeja et al. 2009, from here on Paper I) we applied a cluster analysis based on the nearest-neighbor density method and we identified ten individual PMS stellar clusters in the region. We established that NGC 346 is a multi-clustered environment. This work also provided evidence of hierarchy in the PMS stellar clustering from a graph theory study with the minimum spanning tree and the analysis of the $\mathcal{Q}$ parameter (Cartwright & Whitworth 2004). While these methods provided a unprecedented insight of the NGC 346 clustering, they were not able to quantitatively describe its complexity, or to characterize its self-similar behavior. In addition, the accuracy of the $\mathcal{Q}$ parameter in interpreting a fractal structure has been challenged on the basis of the effect of projection in elongated star clusters (see Bastian et al. 2009 and Cartwright & Whitworth 2009 for different accessions and viewpoints to the problem). The $\mathcal{Q}$ parameter for the whole complex of NGC 346 was found equal to about 0.8, and thus cannot be used to conclude about the nature of stellar clustering in this region.

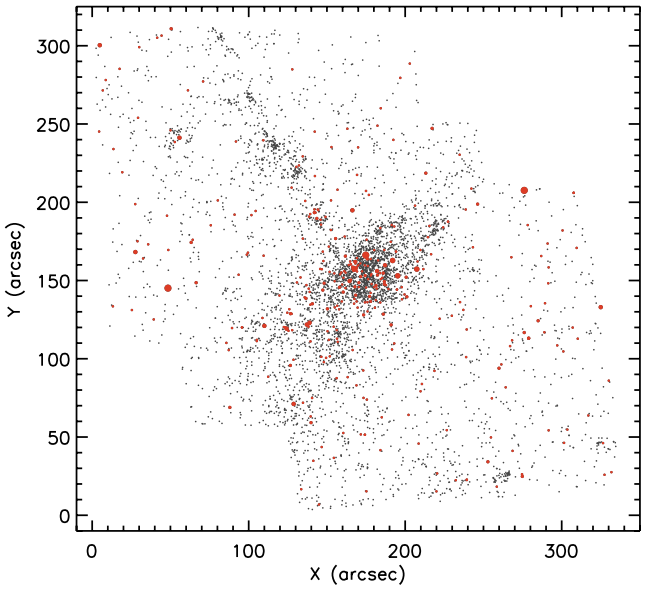

Figure 1. Map of the stars selected for our analysis, i.e., low-mass PMS and more massive upper–main-sequence (UMS) stars, as found in both F555W and F814W filters with DOLPHOT photometry (Dolphin 2000) based on ACS/WFC imaging of three pointings on the field of NGC 346. Red dots correspond to the UMS stars. The map covers the whole observed area. North is up, and east is to the left. Coordinates are given in seconds of arc in respect to a reference point, and are determined based on the drizzled ACS image in the F814W filter.

We revisit the question of stellar clustering in NGC 346 with the application of a thorough cluster analysis. We first assess the topology of young stellar clustering in the region with the kernel density estimation technique, and the distribution function of stellar separations. We then decipher the clustering behavior of young stars in NGC 346 with the construction of their observed two-point correlation function, i.e., their autocorrelation function and its comparison to those from a series of simulated stellar distributions. We explore, thus, the limitations of this method and provide an accurate interpretation of the observed autocorrelation function. We, thus, carefully characterize the complex clustering behavior of young stars in NGC 346.

The paper is organized as follows. In Section 2 we present the stellar surface density map of NGC 346, and the distribution function of stellar separations. In Section 3 we present the autocorrelation function and discuss the first observable evidence that NGC 346 contains (at least) two components with very distinct distributions. We compare the autocorrelation function of NGC 346 with simulations of centrally condensed and self-similar stellar distributions in Section 4. We show that indeed the stellar distribution in the region is the result of two individual stellar components, a central condensed and an extended fractal distribution. In the same section we also constrain the basic parameters of these components using dedicated simulations of mixed stellar distributions. Finally, in Section 5 we summarize our results and discuss their implications to our understanding of clustered star formation. Concluding remarks of our study are given in Section 6. Additionally, in Appendix A we present our library of simulated autocorrelation functions to be used for the interpretation of that observed in NGC 346, and in Appendix B we provide an empirical calibration between

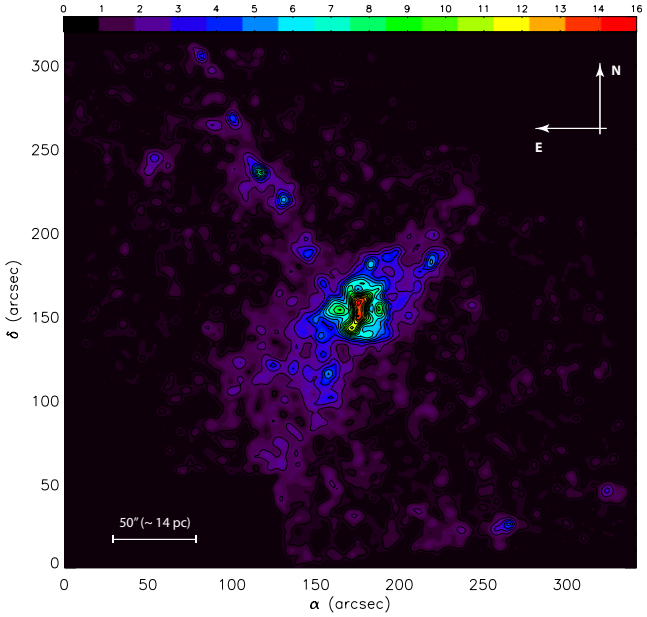

Figure 2. The surface stellar density (significance) map constructed from the sample of young stars in the region of NGC 346 with the use of the KDE technique and a 5″ Gaussian kernel. Isopleths at different density levels, drawn with different colors, signify the individual stellar clusterings identified in this region. The color-bar indicate different density levels in σ, the standard deviation of the measured stellar density in the whole region. North is up and East is to the left. Coordinates are given as in Figure 1.

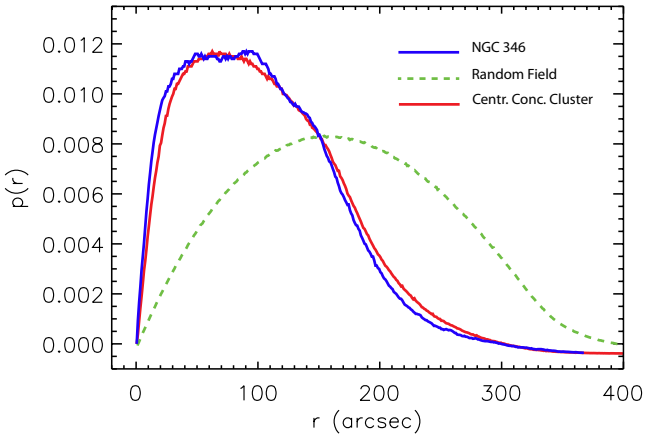

Figure 3. Distribution function for separations between the young stars in our sample for NGC 346 (blue line). The separations distribution $p(r)$ for a simulated field of stars with uniform surface-density (i.e., random distribution; green-dashed line), and that for a centrally concentrated cluster with density gradient $\propto r^{-1.7}$ (red line) are plotted for comparison. The construction of both these artificial stellar distributions are discussed in detail in Appendix A. The separations distribution for NGC 346 shows multiple maxima, and its shape is very close to that for the centrally concentrated cluster (see Section 2.3, for a discussion on this similarity).

three-dimensional and two-dimensional fractal dimensions over a wide range of values.

2 THE SPATIAL DISTRIBUTION OF YOUNG STARS

2.1 The Kernel Density Estimation Map

We construct the surface density map using the *kernel density estimation* (KDE) technique (Silverman 1992). This technique smooths individual data point locations with Gaussian kernels to form a continuous spatial distribution. The fundamental parameter is the full-width-at-half-maximum (FWHM) of the kernel. For the purposes of our study the selection of this parameter was based on the desired 'resolution', i.e., the smallest stellar structure to be identified.

Based on the sizes of the detected stellar clusterings in Paper I, we optimize the construction of the surface density map with a FWHM $\sim 5''$ (equivalent to ~ 1.5 pc)[1]. The produced KDE density map of NGC 346 is shown in Figure 2. In this map small stellar clusterings, coinciding with the stellar groupings previously detected using the nearest-neighbor method, appear as over-densities at density levels of $\gtrsim 2\sigma$. However, all these clusterings are part of a large stellar structure at the 1σ density level. At the lowest, $\sim 1\sigma$ significance level, two large loose stellar over-densities are apparent in the KDE map, which coincide with features that can also be discerned in ionized gas and PAH emission: 1) The central "bar" of the star-forming region, i.e., the bright emission region, extending from southeast to northwest (Rubio et al. 2000), and 2) the "northern arc-like arm" identified in mid-infrared wavebands to extend from the center of the region to the center-northeast part of the field (Gouliermis et al. 2008).

The KDE map of the region depicts, similarly to the nearest-neighbor map, that the region of NGC 346 includes several separate clusterings, defined by the 2σ and 3σ isopleths, characterized in previous studies as individual sub-clusters (Sabbi et al. 2007, Paper I). However, the KDE map illustrates in a far more meticulous manner another critical characteristic of the stellar clustering in NGC 346. There are several compact stellar clumps, which do not appear to be independent, but they emerge as small over-densities within the NGC 346 bar and northern arm. The bar itself is revealed as a large stellar structure (aggregate) in the KDE map at 2σ significance. Stellar distribution within this aggregate is organized in a segregated fashion with the small compact clusterings surrounding a central massive cluster, which appears circular at $\sim 4\sigma$ significance and higher (Figure 2). Whether there is any hierarchy in the manner the aggregate is assembled, whether the central cluster is indeed centrally concentrated and how all the over-densities are connected to each other within the same large structure, are the questions we intend to explore with our analysis.

2.2 Stellar Separations Distribution Function

We derive the probability distribution function of stellar separations for the stars in our sample, following the recipe of Cartwright & Whitworth (2004). The probability function, $p_i(r_j)$, for each star i is calculated as the number of pair separations N_{ij} that fall in the separation bin centered on r_j divided by the total number of separations:

$$p_i(r_j) \quad = \quad \frac{2\,N_{ij}}{N\,(N-1)\,dr}\,, \qquad (1)$$

[1] In Paper I we applied an unsupervised cluster detection, based on the 20th nearest-neighbor density map of the region.

where N is the total number of stars. The distribution function $p(r)$ is calculated in every separation bin from the sum of $p_i(r_j)$:

$$p(r_j) \quad = \quad \sum_{i=1}^{N} p_i(r_j). \tag{2}$$

The probability that the projected separation between two randomly chosen stars is in the interval $(r, r+dr)$ is given by $p(r)dr$.

The separations distribution function for the young stellar population in NGC 346 is presented in Figure 3 (blue line). We also show the stellar separations distribution for a uniform (not clustered) stellar field (green-dashed line), and that for a simulated centrally concentrated cluster (red line). Details on the simulations are discussed in Appendix A. Perusal of Figure 3 shows that overall the separation distribution compares quite well with that of the centrally concentrated cluster with surface density profile $n \propto r^{-1.7}$. However, this agreement is surprising, since evidently both the observed stellar chart (Figure 1) and surface density map (Figure 2) exhibit more structures than can be explained by a simple spherical cluster. This similarity is further discussed in terms of the radial stellar density profile in Section 2.3.

The observed probability distribution also displays a number of local maxima, which indicates the existence of some preferred length-scales in NGC 346, perhaps resulting from multiple clustering in the region. The clearest local maxima occur at separations of about $50''$and $100''$(~ 14 pc and 28 pc respectively). The smaller of these scales coincides with the size of a central stellar concentration, as revealed in the KDE map of Figure 1 at 3σ significance. The maximum at the larger length-scale concurs with the average size of the stellar aggregate in the NGC 346 bar (at 2σ in the KDE map).

2.3 Describing NGC 346 as a single condensed cluster

Based on the stellar separation distribution function, presented in the previous section, one might be tempted to interpret the entire stellar distribution of NGC 346 as originating from a single, centrally concentrated cluster, in spite of the obvious asymmetries in the stellar map. We performed a typical analysis by constructing the radial surface density profile of young stars in the entire observed area, centered on the peak surface density. This profile is shown in blue in Figure 4 (left panel). We then fitted to the observed profile a model cluster density profile with the functional form prescribed by Elson, Fall & Freeman (1987, see Appendix A2.2). The best-fitting model is also shown in Figure 4 (left) in red.

Considering that NGC 346 is certainly not a single condensed cluster, its radial profile was surprisingly well reproduced by models for clusters with core radii of $r_c \simeq 14.9'' \pm 0.7''$, and density profile slopes of $\gamma \simeq 1.69 \pm 0.06$. Such a model cluster is used for comparing the stellar separations distributions shown in Figure 3. This agreement shows that caution is warranted when interpreting radial density profiles, as well as stellar separations distribution functions, in particular in cases where the observations do not allow to recognize prominent asymmetries. It demonstrates the need for a diagnostic tool for stellar distributions, which is equally sensitive to structure afar from the regions with the highest stellar density. To this end we use the two point correlation (autocorrelation) function. The diagnostic power of this function is demonstrated in Figure 4, right panel, which shows that the best-fit cluster distribution fails completely to reproduce the observed autocorrelation function (see Section 4.1), in spite of the excellent fit to the radial profile (Figure 4 left) and stellar separations distribution function (Figure 3).

3 THE AUTOCORRELATION FUNCTION OF YOUNG STARS IN NGC 346

The degree of clustering of stars can be quantified by using the two-point correlation function (Peebles 1980, Section 45). Applied to stars in the same sample, this function becomes an *autocorrelation function* (ACF). In the following, we broadly follow the method introduced by Peebles (1980) for cosmological applications and modified by Gomez et al. (1993) for characterizing the clustering behavior of T Tauri stars in Galactic star-forming regions. Other recent investigations applied this method to observed samples of star clusters in remote galaxies (e.g., Zhang et al. 2001; Scheepmaker et al. 2009, in the Antennae and M 51 galaxies respectively).

The ACF is defined as:

$$1 + \xi(r) \quad = \quad \frac{1}{\bar{n}N} \sum_{i=1}^{N} n_i(r), \tag{3}$$

where $n_i(r)$ is the number density of stars found in an aperture of radius r centered on, but excluding star i. N is the total number of stars and $\bar{n}$ is the average stellar number density. The corresponding uncertainties based on Peebles (1980) are given by:

$$\delta(r) \quad = \quad \sqrt{N} \cdot \left(\frac{1}{2} \sum_{i=1}^{N} n_{\rm p}(r) \right)^{-1/2}, \tag{4}$$

where $n_{\rm p}(r)$ is the number of pairs formed with the central star i of the current aperture, and the factor $1/2$ accounts for not counting every pair twice.

In general, $\xi(r)$ is defined such that $\bar{n}[1 + \xi(r)]d^2r$ is the probability of finding a neighboring star in a area of radius r from a random star in the sample. This means in effect that $1 + \xi(r)$ is a measure for the mean surface density within radius r from a star, divided by the mean surface density of the total sample (i.e. the surface density enhancement within radius r with respect to the global average). Therefore, for a random stellar distribution $1 + \xi(r) = 1$, while for a clustered distribution $1 + \xi(r) > 1$.

For a hierarchical, or fractal, distribution of stars the ACF yields a power-law dependency with radius of the form $1 + \xi(r) \propto r^{\eta}$ (Gomez et al. 1993). For such a distribution, the total number of stars N within an aperture of radius r increases as $N \propto r^{\eta} \cdot r^2 = r^{\eta+2}$. The power-law index η is related to the two-dimensional fractal dimension D_2 as $D_2 = \eta + 2$ (Mandelbrot 1983). Power-law ACFs have been observed for interstellar gas over a large range of environments, and have been interpreted as indications of hierarchical structuring of the gas. The derived typical (three-dimensional) fractal dimension of $D_3 \sim 2.3$ (e.g. Elmegreen & Falgarone 1996; Elmegreen & Elmegreen 2001) apparently comes from the same underlying distribution as found for extragalactic star-forming regions in NGC 628 with a two-dimensional fractal dimension of $D_2 \simeq 1.5$ (Elmegreen et al. 2006). However, the conversion $D_2 = D_3 - 1$ is not generally valid is discussed in Elmegreen & Falgarone (1996) and (Elmegreen & Scalo 2004). In Appendix B we calibrate this relation over a large range of fractal dimensions.

3.1 The Effect of Limited Observed Field-of-View

The ACF, calculated according to Eq. (3), is sensitive to the size of the surveyed area, because apertures around stars close to the edge fall partly outside the survey area, measuring a too low average stellar surface density. This introduces a very steep decrease, dropping well below unity for larger separations due to missing stars out-

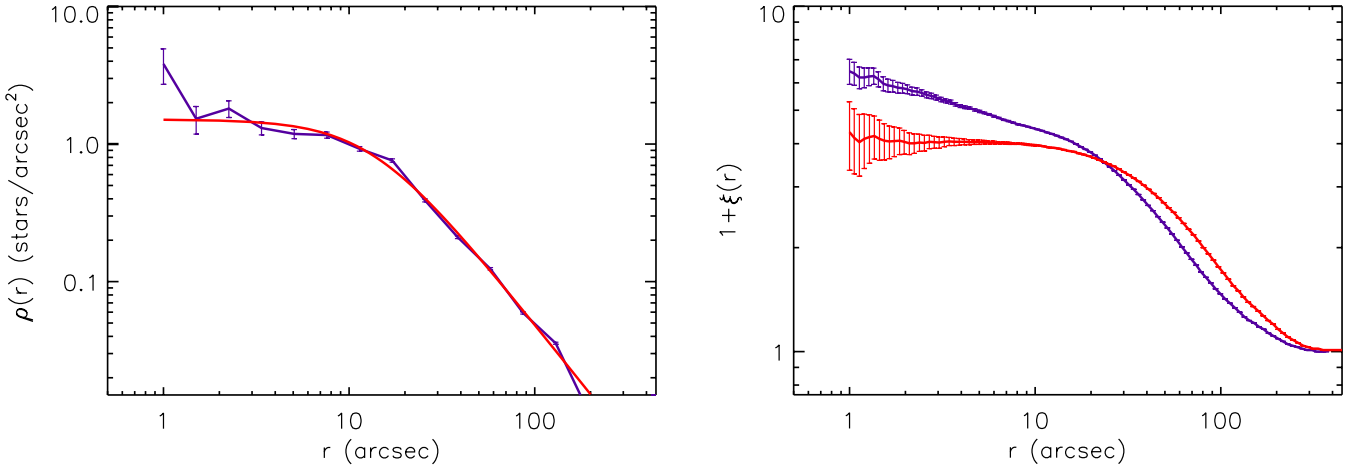

Figure 4. Left: Radial stellar surface density profile of the young stars in the observed field of NGC 346 (in blue). This profile, constructed in concentric annuli, is being build for a first assessment of the structural parameters of the stellar cluster that would best represent the stellar distribution in NGC 346. The best fitting profile model with core radius $r_c \simeq 15''$ and density profile slope $\gamma \simeq 1.7$ is plotted in red. Right: The autocorrelation function of the young stars in NGC 346 (blue) and that of a simulated cluster (red) with the characteristics of the best-fitting model for the observed density profile. The differences between the two autocorrelation functions are striking, demonstrating that the clustering of stars in NGC 346 cannot be explained as being produced by a single centrally concentrated cluster, in contrast to what the radial stellar density profile implies. The right panel is discussed thoroughly in Section 4.1. It is shown here to demonstrate the disagreement in the results between the autocorrelation function and the density profile analyses.

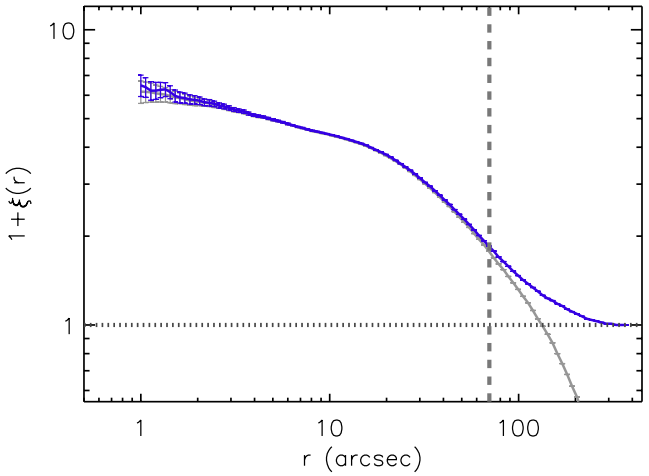

Figure 5. The ACF of the young stellar population (PMS and UMS stars) in NGC 346. The horizontal dashed line corresponds to the ACF of a random field and equals unity. The grey line corresponds to the ACF uncorrected for edge effects, while the blue line depicts the corrected ACF (see discussion in Section 3.1.

side of the observed field-of-view. This behavior is demonstrated in the ACF of NGC 346 shown with a grey line in Figure 5 (described in Section 3.2). The correct way of dealing with this issue is by "masking" the apertures, i.e., by dividing only the part of each aperture that overlaps with the observed field-of-view when calculating average surface densities (n_i in Eq. 3). With this correction the ACF drops smoothly to the level of the random field for larger separations (blue line in Figure 5). From Figure 5 we assess that the correction for the ACF of NGC 346 becomes dominant at separations larger than $\sim 70''$. We consider this ACF, as well as all ACFs simulated in our analysis, to be reliable for separations up to this limit.

3.2 The Observed ACF of NGC 346

The ACF for the young stellar population of NGC 346, constructed according to Eq. (3), is plotted with respect to projected stellar separations in Figure 5. Error bars are determined according to Eq. (4). The clustering of young stars in NGC 346 becomes stronger, i.e., larger values of $1 + \xi(r)$, at smaller stellar separations. This figure also shows that the stellar clustering in NGC 346 changes behavior at different scales. Two distinct parts in the ACF plot can be distinguished at the separation of about $20''$ (~ 5 pc). Both parts show an almost linear decrease of the ACF with radial distance, but with significantly different slopes. Each of these power-law dependencies is similar to that expected for a fractal stellar distribution. However, a purely hierarchical stellar distribution exhibits a single-slope increase of $1 + \xi$ with smaller separations over all scales unlike the ACF of Figure 5 that shows a clear break.

We verify that the ACF of young stars in NGC 346 is well-described by a broken power-law, and we determine its slopes, η, by fitting such a power-law function. We establish the indexes of the two corresponding linear parts by applying a Levenberg–Marquard nonlinear least square minimization technique (Levenberg 1944; Marquardt 1963), as implemented in IDL by Markwardt (2009). The two power-law slopes in the ACF, as well as the position of the break point along the abscissa are the free parameters in our fit. The break in the slope occurs at separations of $20.85''$ (~ 5.8 pc). The inner part ($r \lesssim 21''$) has a power law index $\eta_{\rm in} \simeq -0.18$, which corresponds to a 2D fractal dimension of $D_2 \simeq 1.8$. For separations $21'' \lesssim r \lesssim 70''$ (6 pc $\lesssim r \lesssim$ 20 pc) the ACF has a power-law index of $\eta_{\rm out} \simeq -0.58$ ($D_2 \simeq 1.4$). As we discussed earlier, separations beyond the limit of $\sim 70''$ cannot be considered in our analysis, since at these separations the ACF correction for the finite observed field is dominant.

The fractal dimension found for the small stellar separations in NGC 346 is quite close to the geometrical 2D dimension, suggesting a smooth stellar distribution at these scales. It is interesting to note that at larger scales the derived smaller fractal dimension suggests a more clumpy distribution of stars. This fractal dimen-

sion of $D_2 \simeq 1.4$ agrees very well with that found by several authors for the interstellar gas in the Milky Way and other galaxies (e.g., Falgarone et al. 1991; Westpfahl et al. 1999; Kim et al. 2003), as well as with that found for stellar clusters in external galaxies (e.g., Zhang et al. 2001; Elmegreen et al. 2006; Scheepmaker et al. 2009), and for young stars in several dwarf galaxies (Odekon 2006). These investigations argue that the derived fractal dimensions originate from the turbulent motions in the ISM.

Projected fractal dimensions with values between $D_2 = 1.3$ and 1.5 are considered to be consistent with analogous measures of the 3D fractal dimension of $D_3 \sim 2.4$ derived by both fractional Brownian motion simulations (see, e.g., Stutzki et al. 1998) and from laboratory or numerical turbulent flows (Mandelbrot 1983; Sreenivasan 1991; Federrath et al. 2009). It should be noted that this argument is valid only when the simple conversion $D_3 = D_2 + 1$ holds. Based on our simulations of self-similar stellar distributions (see Appendix A3), we show that *the conversion* $D_3 = D_2 + 1$ *is not generally valid* (see Appendix B). We also establish an empirical relation between the original D_3 used for constructing the distributions and the D_2 values derived with the use of the ACF.

Our findings on the ACF of NGC 346 clearly suggest that stellar clustering at scales larger than $\sim 21''$ is hierarchically driven by turbulence and thus related to the structure of the ISM. Our simulations of fractal distributions, discussed in Appendix A3, show that indeed hierarchical stellar clustering produces a linear dependency of ACF in log-log, but this dependency extends with the same index η across the whole considered length-scales range. Cases where this has been observed are reported by Gomez et al. (1993), Larson (1995), and Simon (1997) in star-forming regions of the Milky Way. The fact that the ACF of Figure 5 behaves like a broken power-law implies that the stellar distribution in NGC 346 is neither a purely hierarchical, nor a pure centrally condensed distribution. In fact, the clear change of slope in the observed ACF provides a strong indication that there are multiple components present, whose distribution is quantitatively and significantly different. The first, high density, component – e.g., a centrally concentrated cluster – affects preferentially the most populated regions of the observed field, while the second, more extended component has significant members throughout the region. This is consistent with the observation that the bar of NGC 346 is a loose stellar congregate, with a definitive compact stellar concentration at its center (Figure 2).

We test the two-components hypothesis by a simple experiment. We repeat our calculation of the ACF while excluding the central compact part of the observed field. Specifically, we mask the stellar sample at significance levels varying between 3 and 8σ from the KDE map of NGC 346 (Figure 2). We find that for values between 5 and 7σ the resulting ACF is very close to a single power law, with an exponent of ~ -0.2. The derived ACF for masking value of 6σ is plotted in red in Figure 6. For higher values of σ, too many stars in the central compact part are retained and the corresponding ACF still exhibits the characteristic break. This experiment provides more confidence that indeed NGC 346 is the conjugated result of two different stellar distributions. The following section is dedicated to obtaining quantitative constraints on the nature of these separate components through numerical simulations.

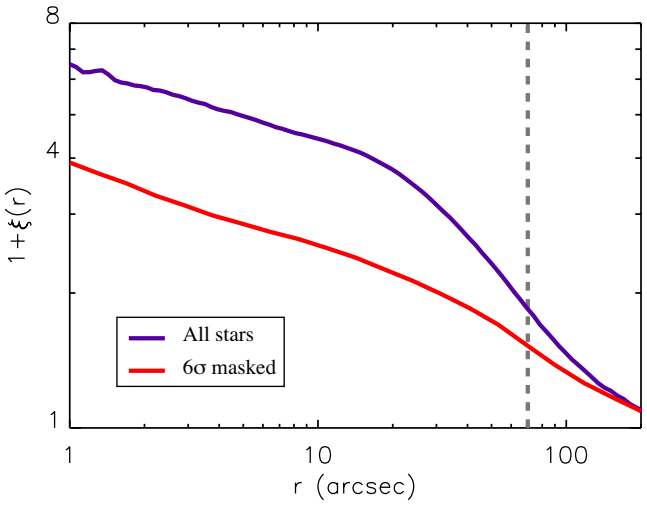

Figure 6. The ACF of the young stellar population in NGC 346 through its complete extend (in blue) compared to the ACF of the same population with the central compact region masked. The ACF derived after masking the stellar sample at 6σ KDE-significance is plotted in red. This ACF exhibits a single slope in contrast to the broken power-law observed for the whole sample. This supports the interpretation that the stellar distribution in NGC 346 is governed by two components, a compact and an extended one. The vertical dashed line indicates the separation of $70''$ beyond which the effect of finite field-of-view becomes dominant.

4 NUMERICAL SIMULATIONS

We derive the nature of the components that dominate the stellar clustering by performing a thorough set of numerical simulations. These simulations are essential for the correct interpretation of observed ACFs, and quantify the uncertainties of the derived clustering parameters. In Appendix A we present a library of ACFs on the basis of simulations of centrally condensed and self-similar stellar distributions. These simulations aid the interpretation of the ACF assuming a *single* type of clustering (compact or fractal). Here we discuss simulations directly applicable to NGC 346, which shows a more complicated clustering behavior with the co-existence of *multiple* stellar components. All considered simulations contain the same number of stars as observed in NGC 346 in comparable field-of-view. This implies that an applicable simulation should reproduce not only the shape of the observed ACF but also the absolute values.

4.1 Simulations of a Single Centrally Condensed Cluster

In Section 2 we found that both the stellar separations distribution function (Figure 3) and the stellar surface density profile of young stars in NGC 346 (Figure 4) imply that the young stars are mostly distributed in a centrally condensed fashion. Therefore, the simplest possible model to describe the ACF of NGC 346 would consist of a single, centrally concentrated cluster. In Appendix A2, among the considered types of centrally condensed cluster models, that proposed by Elson, Fall & Freeman (1987, from hereon the EFF model) is the most appropriate, since it refers to non-tidally truncated clusters like those found embedded in star-forming regions.

We simulated an EFF cluster whose density profile fits best that of NGC 346 (shown in Section 2.3) and constructed its ACF. We compare the ACF of NGC 346 to that of this cluster in Figure 4 (right panel). In this figure, it can be seen that while the density profiles fit very well, the corresponding ACFs are strikingly different from each other. At smaller separations the trend of $1+\xi(r)$ cannot be reproduced by the ACF of the EFF cluster, because it is flat. The decrease of $1+\xi$ with separation for larger scales with index -0.4 does not reproduce that found for NGC 346 (-0.6; Section 3.2) ei-

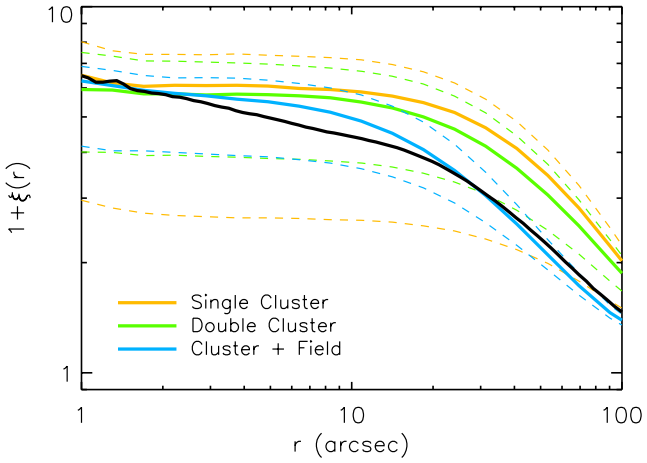

Figure 7. The 'most successful' ACFs of stellar distributions, constructed according to the scenarios discussed in Sections 4.1 - 4.3. We show the results for a single cluster (orange line), a double cluster (green line) and a cluster in a homogeneous field (blue line). They all fail to explain the observed ACF (shown with the black line). We demonstrate the spread in these simulations by also showing, in dashed lines, the results after changing the density profile index of the considered clusters by $\gamma = \pm 0.2$. Even the 'best' simulations of those that do not include a self-similar stellar component fail to reproduce both the shape and absolute values of the ACF of NGC 346.

ther. This result highlights the fact that while the surface density profile of a stellar concentration may give the impression of a centrally concentrated cluster, its ACF may clearly indicate that this is not the case. As a consequence the use of surface density profiles for characterizing uncertain stellar distributions (e.g., open clusters and loose stellar groups) should be made with caution, as it may not represent reality.

We explored the possibility that other EFF clusters may reproduce the observed ACF, but we found that *all* simulated EFF profiles fail to reproduce the main characteristics of the observed ACF. They all produce constant $(1 + \xi)$ values at scales smaller than their core-radii, not agreeing with the observed ACF of NGC 346 at these scales. In particular, those clusters that had stellar densities at shorter separations compatible to that of NGC 346 contained unrealistically large numbers of stars within their core radii. The ACF of the "most successful" set of our simulations of a single centrally condensed cluster is plotted in Figure 7 (orange line), where it is shown that the single-cluster scenario cannot reproduce successfully the observed ACF. From this analysis we conclude that while the stellar density map of NGC 346 indicates the existence of a condensed stellar cluster, the ACF indicates that not all young stars in NGC 346 can belong to the central cluster and thus another, more extended, component should be also considered. This result is additionally supported by the decomposed ACF of NGC 346 (Figure 6), constructed by masking the central condensed cluster

In the following sections we explore the constraints we can obtain on the nature of this extended component. We identify the type of this component by applying simulations of the combination of two individual stellar distributions. The total number of stars and the field-of-view in these simulations are again identical to the observed ones in NGC 346. The basic input parameters in our experiments are (1) the fraction of stars with respect to the total considered number that belong to each component, (2) the core radii and γ indexes of each considered condensed cluster, and (3) the fractal dimensions of the simulated self-similar distributions.

4.2 Simulations of two Centrally Condensed Clusters

We study the possibility of reproducing the main characteristics of the observed ACF, assuming two centrally condensed stellar components. This is motivated by the fact that in the stellar surface density (KDE) map of Figure 2 a small number (< 4) of isolated density peaks can be seen, depending on the chosen significance level. We produced mock stellar catalogs with the addition of two EFF clusters, with a total number of observed stars equal to that of NGC 346 (5,150 stars). We produced a grid of combinations in the stellar distribution by varying the following parameters: 1) Projected separation between the clusters, which varied from $10''$ to $25''$, 2) the fraction of stars belonging to the first cluster (0.5 to 0.7), 3) the EFF profile indexes γ (between 1.6 and 2.2), and 4) the core radii, r_c, which was set between $6''$ and $12''$.

The best correspondences between models and observations were found for low values of γ ($\sim$1.8) and core radii (~ 8 - $10''$). Distributing the stars in roughly equal amounts over two clusters allows for somewhat smaller individual clusters, which alleviates to some extent the problem of having too many stars within the core radius – and thus absolute ACF values higher than the observed. This is demonstrated in Figure 7, where the most well representative ACF from our simulations of two centrally condensed clusters is shown (in green). If the separation between the clusters is tuned to be roughly consistent with the observed break of about $21''$, the smaller clusters combined can still yield a weak break at this separation in the ACF, but cannot reproduce the power-law trend of the observed ACF at scales below $15''$. In general, all of the considered combinations of two EFF clusters completely failed to reproduce the behavior of the ACF of NGC 346 in the complete range of separations.

4.3 Simulations of a Single Cluster plus a Homogeneous Field

One of the striking features of the distribution of the young population in NGC 346 is that there are stars found distributed throughout the observed region (see also Paper I), which may be an indication of a truly dispersed population, i.e., a (young) background field population. We simulate thus clusters that are located within a homogeneous field. In these simulations we vary the following parameters: 1) The fraction of stars that belong to the EFF cluster ($f_{\rm cl}$: 0.4 to 0.7), 2) the core radius ($3''$ - $15''$) and 3) the slope γ (1.5 - 3.0) of the cluster profile.

The best agreement with the observed ACF is found for $f_{\rm cl} \simeq 0.5$, core radii between $8''$ and $10''$and quite high γ values from 2.2 to 2.5. For these parameters the peak stellar surface density (i.e., the ACF values at the smallest separation bin) and the ACF at separations larger than $21''$ are well reproduced. However, all simulated distributions fail to reproduce the ACF behavior at separations smaller than $15''$, in identical manner as the two previous scenarios (see Figure 7). The origin of this general mismatch with the observations is the fact that the stellar surface density of both the underlying EFF distributions and the random field does not increase at continuously smaller spatial scales.

4.4 Simulations of a purely Self-Similar Distribution

In Appendix A3 we present a detailed account of the behavior of the ACF for self-similar, i.e. fractal, stellar clusterings, based on artificial stellar distributions. It is shown that hierarchical stellar distributions are characterized by a monotonous (i.e. single-slope) linear

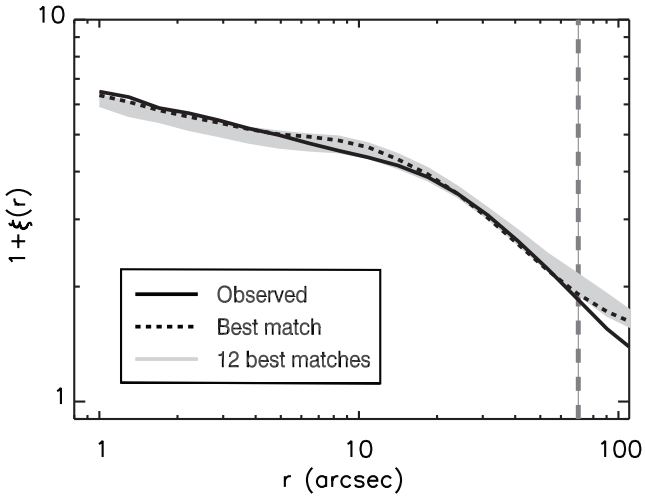

Figure 8. The observed ACF of NGC 346 (solid black line) with the area filled by the ACFs of the best-representative simulated mixed distributions that assume a central compact stellar component and an extended fractal one (light grey). The useful separations range of $\lesssim 70''$, where the ACF indexes were determined, is indicated by the vertical dashed line. These models succeed in reproducing the observed ACF at the shortest and longest stellar separations. They have, though, the tendency to over-predict the ACF values at separation of $\sim 10''$. The ACF of the best-matching model is plotted with a short dashed line. These simulations provide constraints for the basic parameters of the contributing stellar distributions, with the central cluster having a core radius of $\sim 9''$(~ 2.5 pc) and extending with a slope $\gamma \sim 2.27$, and the self-similar distribution having a fractal dimension of $D_3 \sim 2.3$.

dependency of the ACF on stellar separations in log-log, which extends across the whole considered length-scales range. The shape of the observed ACF for NGC 346 (Figures 5 and 6) is proven to behave like a broken power-law with different slopes for different separations ranges (Section 3.2). As a consequence, with our simulations of pure fractal stellar distributions we are able to reproduce each one of the two linear parts of the observed ACF, but not its complete shape across the whole separations range. As we discuss in Section 3.2, and show in the following section, a second stellar component must be considered in order to successfully reproduce the broken power-law behavior of this ACF.

4.5 Simulations of a Single Cluster plus a Self-Similar Distribution

The decomposed ACF of Figure 6, constructed by masking the central condensed stellar concentration of the region, strongly suggests the existence of an underlie self-similar distribution of young stars in NGC 346, and it provided the first evidence that the system may be the combined result of two such diverse stellar distributions. Indeed, we find that the most successful simulations in replicating the observed behavior of ACF for NGC 346 are those which contain both a centrally concentrated dense cluster and a large-scale hierarchical (fractal) distribution.

We constructed a sample of distributions by varying the following parameters. (1) The fraction of stars that belong to the cluster $f_{\rm cl}$ (between 0.3 and 0.7), the core radius of the EFF cluster ($7''$ - $12''$), the γ index of its profile (1.8 - 3.0) and the three-dimensional fractal dimension D_3 of the fractal distribution (from 2 to 2.6). There is only a small subset of these models that is able to reproduce satisfactorily that observed ACF, i.e. the peak value of $1+\xi$, the power-law slope for separations between $1''$ and $21''$, and the steeper slope for larger separations ($21''$ to $70''$). The simulations that represent best the observed ACF have 2,300 to 2,500 stars in the cluster, which has a core radius of $4''$ to $9''$ and γ between 2.25 and 2.35. The best-matching extended component has a high fractal dimension ($2.2 < D_3 < 2.4$). Smaller clusters systematically over-predict the ACF peak value (at the shortest-scale bin). Clusters with core radii $\gtrsim 10''$fail to simultaneously reproduce the AVF behavior at both small and large separations. They produce too much correlation for large separations, which can be remedied by increasing the fraction of stars in the cluster but then the power-law behavior at shorter spacings is lost.

With these dedicated simulations we succeeded in reproducing both the shallow linear behavior of NGC 346 ACF at short separations, as well as its steeper drop at large separations. We reproduced the ACF index for every part of its broken power-law, as well as the separation limit, where the break occurs. Twelve of our combined simulations reproduce the ACF of NGC 346, providing constraints to the basic parameters of the assumed stellar distributions. In all these simulations the core radius of the central cluster is found to be practically unchanged and equal to $\sim 8''$ - $9''$. The fraction of stars in the EFF cluster varies around 0.4, and the slope γ of the assumed cluster profile has values $\gamma \simeq 2.20$ to 2.35. Finally, the input three-dimensional fractal dimension of the best-fitting simulations varies at values between ~ 2.20 and 2.36.

The observed ACF of NGC 346 and those of the twelve most successful simulations are shown in Figure 8. It should be noted that the modeled ACFs are very sensitive to the chosen parameters. We established the best-matching models by iteratively refining the input parameters. In Figure 9 the KDE surface density map of the most successful distribution (short dashed line in Figure 8) with $f_{\rm cl} = 0.4$, $r_{\rm c} = 9''$, $\gamma = 2.3$, and $D_3 = 2.32$, is shown to be compared to the KDE map of NGC 346. This density map shows secondary peaks, resembling concentrations seen in NGC 346. Nevertheless, we could not reproduce the amplitude of the second most important stellar clump of NGC 346, which may mean that there is a second (much smaller) compact cluster in the region.

5 SUMMARY AND DISCUSSION

In this study we present a thorough analysis of the clustering behavior of young stars in the star-forming region NGC 346. In particular, we construct the KDE density map and the separations distribution function, and we determine the ACF of the rich sample of low-mass PMS stars (supplemented by the young massive stars) in the region. We show that the ACF is a robust method to characterize the clustering of stars, providing that its behavior is accurately understood through dedicated simulations. We characterize the stellar clustering in NGC 346, and interpret its ACF, through the construction and study of the ACFs of simulated centrally condensed and fractal stellar distributions.

We previously found indications that NGC 346 includes multiple compact stellar over-densities, and that the distribution of PMS stars in the region is hierarchical (Paper I). With our analysis here we demonstrate that the young stellar design of NGC 346 is far more complicated. The comparison of the observed ACF with those of simulated stellar distributions shows clear evidence that NGC 346 includes a hierarchical stellar component, extended across the whole field-of-view, and a compact stellar cluster, which appears more dominant in the central part of the observed region.

The observed ACF of young stars in NGC 346 is successfully

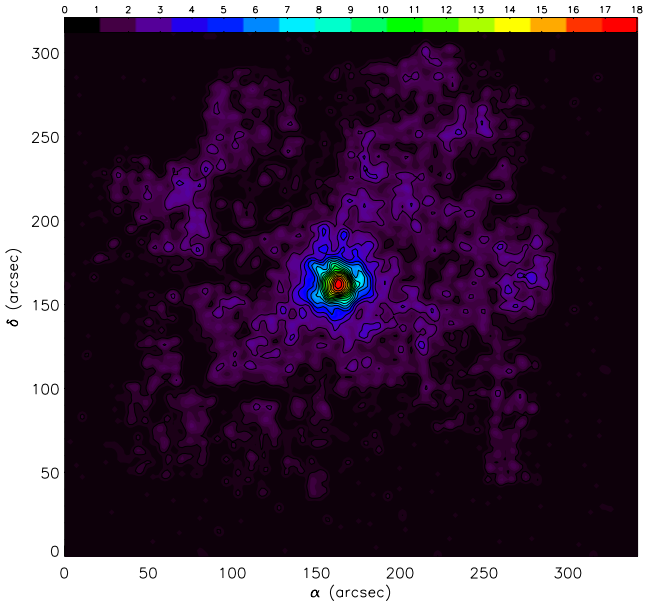

Figure 9. Surface stellar density (significance) map constructed from the synthetic stellar distribution that represents best the stellar clustering in NGC 346. The map is constructed with the use of the KDE technique and a 5″ Gaussian kernel, in comparison to the NGC 346 map of Figure 2. The color-bar indicates different density levels in σ, the standard deviation of the measured stellar density in the regions. The artificial field-of-view is identical to the observed field-of-view. Coordinates are given as in Figure 2 for NGC 346.

reproduced if we assume that $\sim$40% of the stellar population belongs to a condensed cluster with core radius of $r_{\rm c} \sim 2.5$ pc and a density profile index $\gamma \sim 2.3$, "embedded" in a self-similar stellar distribution with a fractal dimension of $D_3 \sim 2.3$. NGC 346 is, thus, a very interesting example of composed stellar distributions, on length-scales typical for molecular clouds, providing an unprecedented insight of the topology of star formation. The fact that we still observe self-similar stellar clustering even after $\sim$3 Myr is also interesting, because this time-scale provides a constraint on how long it takes for the stars to lose their primordial spatial distribution.

The derived three-dimensional fractal dimension of $D_3 \simeq 2.3$, for the self-similar stellar component, fits very well to the value derived from numerical experiments of supersonic isothermal turbulence (Federrath et al. 2009), and with measurements inferred from observations of the interstellar gas (Elmegreen & Elmegreen 2001). This agreement implies that the self-similar stellar distribution in NGC 346 is possibly inherited by the turbulent interstellar gas of the natal molecular cloud. In our study for the determination of D_3 we use the ACF, Federrath et al. (2009) argue that the Δ-variance (Stutzki et al. 1998; Ossenkopf et al. 2008) is the most reliable method, and Elmegreen & Elmegreen (2001) use the size distribution function of stellar aggregates. Although different, all three studies agree in the derived value of $D_3 \sim 2.3$.

On the other hand, recent numerical simulations by Girichidis et al. (2012) and Dale et al. (2013) find a higher degree of hierarchy for stars formed from turbulent molecular clouds with smaller values of $D_3 \sim 1.6$. These studies, which apply the $\mathcal{Q}$-parameter (Cartwright & Whitworth 2004), find similar fractal dimensions with that inferred from the same method for the Taurus molecular complex ($D_3 \sim 1.5$), in line with the fractal dimensions of the ISM in this region (see, e.g., Alfaro & Sánchez 2011).

While the differences in the derived fractal dimensions may reflect discrepancies in the methods used, the may as well demonstrate the fact that stars have a different spatial distribution to the gas from which they formed, or that the gas is not similarly structured everywhere. Observations of nearby Galactic star-forming regions show that while the gas filaments have a smooth, radially decreasing density profile (e.g., Arzoumanian et al. 2011), the distribution of recently-formed stars ($\tau \sim 1$ Myr) has a range of different morphologies, some being fractal and others centrally concentrated (Cartwright & Whitworth 2004).

Whether or not every stellar distribution forms with substructure has yet to be determined. N-body simulations suggest that even a moderate amount of dynamical interactions will partly erase substructure, forbidding a star-forming region from retaining a strong signature of the primordial ISM distribution (e.g., Scally & Clarke 2002; Goodwin & Whitworth 2004). Considering that subsequent substructure is difficult to be formed, and dynamics may have aided the formation of a condensed cluster in NGC 346, the observed substructure may be an upper limit of the primordial value.

The existence of the central compact cluster naturally complicates somewhat the star formation picture in the region. Assuming that the clustered stellar population is coeval with the extended hierarchical stellar component, one has to consider two scenarios for its formation: Either (1) this cluster was formed as a distinct prominent compact concentration amid a distributed stellar population, or (2) it was originally formed as part of the extended stellar component, and soon became centrally condensed due to rapid dynamical evolution.

The first scenario implies the co-existence of two different modes of star formation; one that produces a centrally concentrated cluster plus another that is responsible for the distributed PMS stars. The formation of both clustered and distributed populations of young stars in a single molecular cloud is numerically described by Bonnell et al. (2011), where both modes are determined by the local gravitational binding of the cloud. The bimodal star formation scenario is further supported by the large number of 'unclustered' PMS stars (see also Paper I).

The second scenario assumes that the centrally condensed cluster in NGC 346 is the merging product of distinct compact newly-born sub-clusters within the natal cloud. This scenario is supported by hierarchical fragmentation of the turbulent molecular cloud, which forms stars in many small sub-clusters (Klessen & Burkert 2000). These sub-clusters will interact and merge to form a dominant stellar cluster through closer and more frequent dynamical interactions (Bonnell et al. 2003). The existence of compact PMS sub-clusters along the whole extend of NGC 346 makes this scenario favorable. Recent N-body simulations of the dynamical evolution of star-forming regions by Parker et al. (2013) also support this scenario. In these simulations, initially sub-structured super-virial agglomerations will evolve to form a multi-clustered region, similar to NGC 346, within 5 Myr.

The simulations by Parker et al. (2013) predict that star-forming regions will dynamically evolve to form bound clusters or unbound associations, depending on their initial conditions, i.e., their virial status and fractal dimension. Based on the present status of the central cluster, we cannot know which of the above scenarios explains its origins. Specifically, it is unclear if the cluster is still under formation (through merging or not), and if it is undergoing core collapse that evaporates its low-mass stars due to gas expulsion (Baumgardt & Kroupa 2007), or through rapid dynamical interactions (Allison et al. 2010). Considering that all simulations discussed here deal with length-scales and stellar numbers smaller

than that of NGC 346, modeling of richer stellar samples in larger areas is surely necessary for constraining the initial conditions that led to the formation of NGC 346.

Most simulations predict central segregation of the most massive stars, but they measure it with different methods and explain it with different mechanisms. Mass segregation may be primordial because massive stars are born in situ at the central region, or due to rapid equipartition, and so it is the product of dynamical evolution. Mass segregation is observed in NGC 346 through the comparison of its isochronal age with the time-scale for energy equipartition, i.e., for mass segregation (Spitzer 1987, p. 74, see also Kroupa 2004). Sabbi et al. (2008) found that the latter is one order of a magnitude larger, impliying that the observed mass segregation is likely due to initial conditions, rather than dynamical evolution.

The present dynamical status of whole region of NGC 346 can be naively[2] determined in terms of its relaxation and crossing time-scales. The relaxation time, $T_{\rm relax} \approx (0.1\,N/\ln N)\,T_{\rm cr}$, is the time for significant energy redistribution to occur in a cluster (Binney & Tremaine 1987, p. 37), where $T_{\rm cr} \approx 2r_{\rm h}/\sigma$, is the crossing time of a typical star through the cluster which has a characteristic radius $r_{\rm h}$ and a velocity dispersion $\sigma \approx GM/r_{\rm h}$ (see also Kroupa 2008). $G = 0.0045\,{\rm pc}^3/\left({\rm M}_\odot\,{\rm Myr}^2\right)$ is the gravitational constant, N the total number of stars, and M that total stellar mass of the cluster. Using a radius $r_{\rm h} \simeq 9\,$pc and a total mass $M \simeq 3.9\,10^5\,{\rm M}_\odot$, Sabbi et al. (2008) derives $T_{\rm relax} \simeq 570\,$Myr, far larger than the age of NGC 346. This result, supported by the apparent substructure in the region suggests that NGC 346 is not dynamically relaxed, in agreement with the assumption that mass segregation in NGC 346 is primordial.

Gieles & Portegies Zwart (2011) use the ratio of stellar age over the crossing time, $\Pi = {\rm Age}/T_{\rm cr}$, to distinguish bound from unbound stellar systems, with $\Pi < 1$ for unbound, i.e., expanding, objects. Using their own definition of the crossing time in terms of empirical cluster parameters (their Eq. 1), and the values for age, $r_{\rm h}$ and M from Sabbi et al., they derive $T_{\rm cr} = 6.4\,$Myr, and thus $\Pi \approx 0.5$, classifying NGC 346 as unbound agglomerate. However, assuming a velocity dispersion of $\sigma = 10\,{\rm km\,s}^{-1}$, typical for star-forming complexes of the size of NGC 346, Sabbi et al. derives $T_{\rm cr} = 1.8\,$Myr, which classifies NGC 346 as a bound system.

The difference in the results between the above studies is important, because they influence our understanding of the origin of the region and, thus, the nature of its bimodal stellar clustering. If NGC 346 is a gravitationally bound object, but not relaxed yet, as the findings of Sabbi et al. (2008) suggest, then probably the condensed stellar component is the *undergoing result of dynamical interactions* between smaller clusters. On the other hand if NGC 346 expands as the result of Gieles & Portegies Zwart (2011) implies, then most probably the central cluster *was originally formed condensed*. Under these circumstances a clarification about the origin of the central cluster and of the bimodal clustering behavior of the young stars in NGC 346 can only be achieved with the accurate determination of stellar dynamics, i.e., kinematics, of the region.

By reversing the above analysis we make a prediction for the velocity dispersion that the system would have if it was dynamically stable or unstable. The condition for stability for NGC 346 ($\Pi = 1$) requires $T_{\rm cr} = 3\,$Myr, which implies a velocity dispersion of $\sigma \simeq 6\,{\rm km\,s}^{-1}$ for $r_{\rm h} = 9\,$pc. (This value is in excellent agreement with the line-of-sight velocity dispersion of stars within a projected distance of 5 pc from the centre of the young massive cluster R136 in the Tarantula nebula; see Hénault-Brunet et al. 2012.) It should be noted that the half-number radius, i.e., the characteristic radius, in our young stellar sample is larger than that determined by Sabbi et al., and equal to $r_{\rm h} \simeq 16.5\,$pc. Assuming this radius, the velocity dispersion at the stability limit raises to $\sigma \simeq 11\,{\rm km\,s}^{-1}$, still within typical values (e.g., Sana et al. 2013). The predicted values of 6 - 11 km s^{-1} for the velocity dispersion of NGC 346 provide a limit for characterizing the stability of the system as a whole. If the velocity dispersion is larger that this limit, NGC 346 is bound and collapsing (since $\Pi > 1$), while for values lower than this estimate, the system is unbound, and thus possibly under dissolution. In any case, different stellar components in the region are expected to demonstrate different velocity dispersions, depending on their own dynamical status.

In the above discussion we assume a single age of $\sim 3\,$Myr for the entire region, based on its PMS stars (Sabbi et al. 2008). However, single-epoch photometry of PMS stars is significantly affected by their physical characteristics (unresolved binarity, accretion, circumstellar extinction, variability, etc) that dislocate these stars from their theoretical positions on the color-magnitude diagram. This effect causes a color-luminosity spread of the PMS stars, which translates to an artificial age-spread, making the measurement of stellar ages (and masses) quite uncertain (see review by Gouliermis 2012). This issue, for *Hubble* imaging of PMS stars in the Magellanic Clouds, can only be accurately addressed through probabilistic determination of their physical parameters (e.g., Da Rio et al. 2010). Naturally, a more accurate determination of PMS ages in NGC 346 and verification of an age-spread, which may even be positional dependent, would have noticeable implications to our understanding of star formation in the region.

6 CONCLUDING REMARKS

Concluding remarks, derived from our analysis, are summarized to the following:

Large star-forming complexes are excellent stellar 'ecosystems' for the investigation of clustered star formation, because the represent the typical 100-pc scale of giant molecular clouds.

The combined application of various cluster analysis tools is necessary for thoroughly characterizing young stellar clustering. In particular the autocorrelation function emerges as a robust method, because, supported by the appropriate simulations, it is capable to distinguish different clustering styles.

We determine that the clustering of young stellar populations in the star-forming complex NGC 346 has two distinct components; An extended self-similar, i.e., hierarchical, stellar distribution, and at least a centrally condensed young stellar cluster.

Dedicated simulations of combined stellar distributions show that the condensed stellar component of fits to a spherical cluster, including 40% of the stars, with a core radius between 8″and 9″($\sim 2.5\,$pc) and a power-law surface density profile with slope between 2.20 and 2.35. The remaining population is fractally distributed across the whole extent of the region with a fractal dimension D_3 between 2.20 and 2.36.

Our findings suggest that the present clustering behavior of young stars in NGC 346 is the product of both star formation (turbulent-induced hierarchy), and early dynamical evolution (merging towards or dissolution of a centrally condensed cluster).

[2] Due to its asymmetrical stellar clustering, the determination of a crossing time for the whole region may not make sense. It is, though, useful in understanding its dynamical status, especially in comparison to other objects.

Both processes seem to be still active after a time-scale of ~ 3 Myr, i.e., the assumed evolutionary age of the region.

The origin of this bimodal clustering behavior is not clearly understood. Considering that it influences the future evolution of the region, we assess that if the complete system is under disruption then possibly the central cluster was formed condensed. If NGC 346 contracts under its own gravity then this would imply that the central cluster may be the product of this contraction. We determine that the velocity dispersion limit for stability of the region as a whole is $\sigma \gtrsim$ 6 - 11 km s^{-1}. However, based on the heterogeneous clustering of the region, the *local* velocity dispersion of individual sub-structures should demonstrate variations.

Considering the excellent coincidence of the fractal dimension derived for the stellar clustering with that measured and theoretically predicted for the turbulent interstellar medium, a natural step forward for this study is to understand how the stellar assembling process relates to the structuring behavior of the natal interstellar medium. This topic will be addressed in a subsequent study, where we compare the interstellar gas structure to that presented here for the young stars in NGC 346.

ACKNOWLEDGMENTS

We thank Richard Parker and Stefan Schmeja for their critical views and useful discussions that helped improving our interpretation. D.A.G. kindly acknowledges financial support by the German Research Foundation through grant GO 1659/3-1. S.H. and R.S.K. acknowledge support from the Collaborative Research Center "The Milky Way System" (SFB 881), particularly subproject B5, of the German Research Foundation. Based on observations made with the NASA/ESA *Hubble Space Telescope*, obtained from the data archive at the Space Telescope Science Institute (STScI). STScI is operated by the Association of Universities for Research in Astronomy, Inc. under NASA contract NAS 5-26555.

APPENDIX A: LIBRARY OF SIMULATED AUTOCORRELATION FUNCTIONS

A1 The Requirement for Simulated ACFs

A cluster analysis method, developed by Larson (1995) as a modification of the standard two-point angular correlation function (Gomez et al. 1993), is the correlation of the mean surface density of stellar companions (MSDC) against pair separation (in logarithmic scales). In general, the MSDC behaves in analogy to the ACF[3], with a power-law index η being identically associated to the fractal dimension D_2. Both methods, however, are subject to observational limitations in their interpretation.

A break in the power-law of the MSDC of Galactic star-forming regions is suggested to be strongly influenced by the overall stellar surface density (Simon 1997; Bate et al. 1998), rather than representing a characteristic scale, as was previously proposed. Moreover, a single power-law index may not even be related to the fractal dimension of the clustering, merely reflecting the large-scale density gradient in a centrally concentrated cluster (Bate et al. 1998; Klessen & Kroupa 2001). These limitations, in addition to edge effects introduced by the unavoidably limited observed fields (Cartwright & Whitworth 2004, see also Section 3.1), require the simulation of distinctive stellar clusterings for the correct characterization of the ACF, and its use as a cluster analysis diagnostic.

In this Appendix we build a library of typical ACFs, based on simulations of centrally concentrated clusters and fractal stellar distributions. We describe these simulations and their ACFs in Appendices A2 and A3, where we also verify the behavior of the ACF for a random stellar distribution, i.e., for a sample of non-clustered stars (Appendices A2.1 and A2.2). These 'field' ACFs are consistent with a value of $\simeq 1$, and remain unchanged with the separation range. The spatial coverage and stellar numbers of all considered artificial distributions are scaled to be identical to the field-of-view and stellar sample covered by our *Hubble* ACS observations of NGC 346.

A2 The Autocorrelation Function of Centrally Concentrated Stellar Distributions

We examine the autocorrelation of stars spatially related to each other within a spherically symmetric cluster. We compose artificial centrally-condensed stellar distributions that follow typical stellar surface density profiles, and we construct the corresponding ACFs in order to comprehend their behavior in comparison to the observed ACF of NGC 346. All simulations are performed for the same number of stars with that in our observed sample (5,150) confined within a field-of-view identical to that covered by the three ACS/WFC pointings mosaic. We consider two types of radial stellar density profiles for the synthetic clusters: Profiles following the empirical law by King (1962), and those represented by the model of Elson, Fall & Freeman (1987). The latter, representing clusters that are not tidally truncated, are best-suited for extended clusters surrounded by well populated stellar fields, as is usually the case in large star forming regions like NGC 346. Therefore we base our analysis on these clusters, the simulations of which are presented in Appendix A2.2. Below, we also present the King star cluster profiles for reasons of completion in our study, and for a reference for future studies on the ACF of star clusters.

A2.1 King-profile Clusters

We further investigate the ACF of more realistic centrally concentrated stellar clusters in dynamical equipartition. Artificial spherical clusters were simulated to follow stellar surface density profiles defined by King's semi-empirical model (e.g., King 1962). The functional form of these profiles is:

$$f(r) \quad \propto \quad \Big(\frac{1}{[1+(r/r_{\rm c})^2]^{\frac{1}{2}}} - \frac{1}{[1+(r_{\rm t}/r_{\rm c})^2]^{\frac{1}{2}}}\Big)^2, \qquad \text{(A1)}$$

where f is the stellar surface density, and r is radial distance. The clusters are constructed with various values in their concentration parameter c, defined as $c = \log r_{\rm t}/r_{\rm c}$, where $r_{\rm t}$ and $r_{\rm c}$ are the tidal and core radius of the cluster.

The ACFs for a sample of such clusters are shown in Figure A1 along with that for the random field (plotted in red). Clusters are constructed with concentration parameters equal to 0.5 (plotted in orange), 1.0 (light green), 1.5 (green) and 3.0 (blue) respectively. The latter represents the observed extreme in the parameters space

[3] An advantage of the ACF over the MSDC is that the former is normalized by the average density in the survey area. This allows the clear distinction between strongly and weakly clustered samples (from the absolute ACF values), and the direct comparison of the shape of ACF for different ensembles.

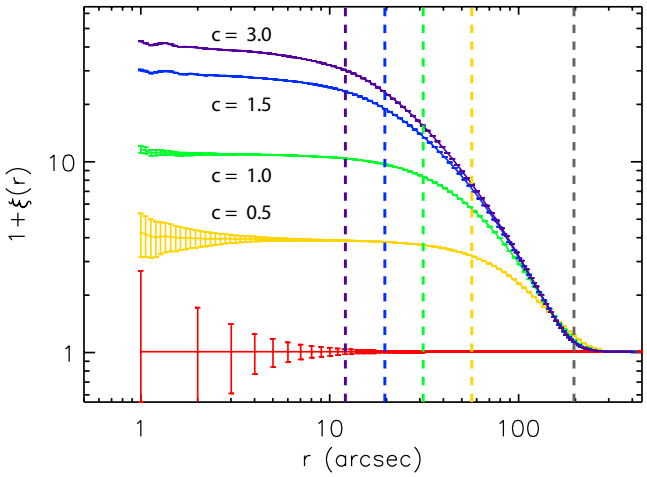

Figure A1. ACFs for a sample of four centrally concentrated clusters that follow King-type stellar density profiles with different concentration parameters, c, as indicated in the plot. Vertical color dotted lines correspond to the $r_{\rm h}$ of the clusters, and the black dashed line corresponds to the $r_{\rm t}$ of the clusters, which is chosen to be identical and equal to 55 pc. The ACF of a random stellar distribution is plotted for reference in red.

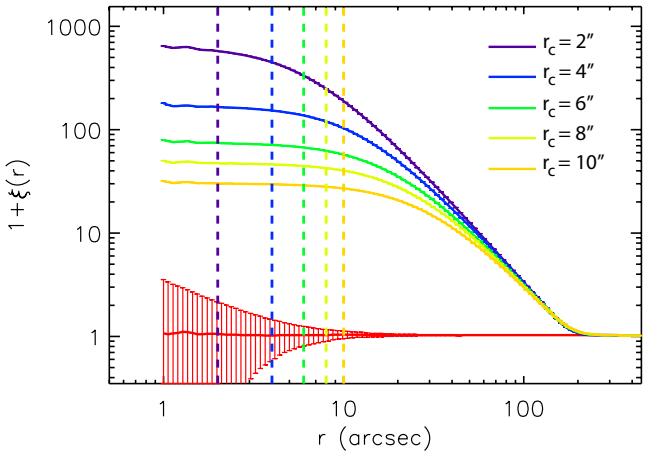

Figure A2. ACFs for a sample of five centrally concentrated clusters that follow EFF-type stellar density profiles. All clusters in the plot have the same number of stars, $\sim 5,000$, and a fixed outer profile slope, $\gamma = 3$, typical for young clusters in the Magellanic Clouds, while their core radii, $r_{\rm c}$, vary. They are selected to have typical values of $2''$, $4''$, $6''$, $8''$, and $10''$, indicated with vertical dashed lines in magenta, blue, green, light-green and orange respectively. The ACF of a simulated random (unclustered) field of the same number of stars is shown in red for reference.

of known Galactic globular clusters (Pal 12, $c = 2.98$; Harris 1996, 2010 Edition[4]). From these plots it is seen that while indeed for all clusters the autocorrelation function is $1 + \xi(r) > 1$, it does not again remain constant through the whole range of stellar separations r, but it drops at larger separations towards the outskirts of the clusters converging to the random field value of unity. The ACFs reach this value at the radii where essentially the clusters meet the surrounding field, comparable to their tidal radii. For reasons of simplicity, in the examples shown in Figure A1 all clusters are constructed to have the same $r_{\rm t} = 55$ pc ($\simeq 196''$).

There are two derivatives from these simulations: (1) The

[4] http://physwww.physics.mcmaster.ca/∼harris/mwgc.dat

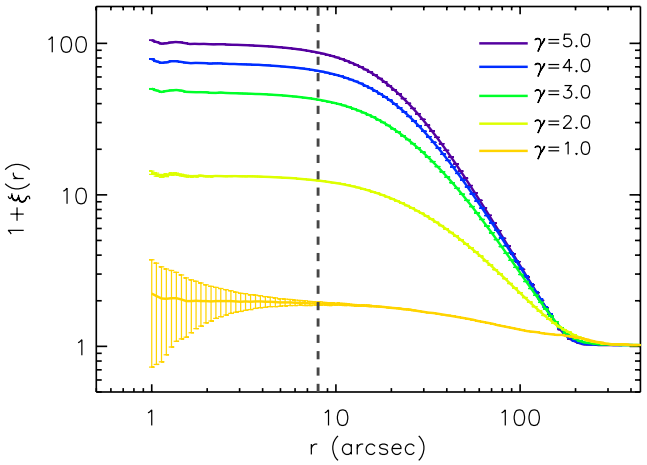

Figure A3. ACFs for a sample of five centrally concentrated clusters that follow EFF-type stellar density profiles. All clusters have the same number of stars, $\sim 5,000$, and a typical fixed core radius, $r_{\rm c} = 8''$, indicated in the plot with the vertical grey dashed line. Their outer density profile indexes, γ, are selected to have values typical for young Magellanic Clouds clusters, of 1, 2, 3, 4, and 5. The case of $\gamma = 1$ is an unobserved extreme used here for demonstrating the flatness of its ACF.

maximum values of $1+\xi$ depend on the degree of concentration, i.e. the concentration parameter, of each cluster; More centrally concentrated clusters have higher ACF values, and they are thus 'more clustered'. This trend, which is more obvious at small separations, becomes less important for clusters with $c \gtrsim 1.5$. (2) The shape of the ACF drops at larger separations (up to the field value) also depends on the concentration parameter. It naturally depends also on the limiting radius of the cluster, i.e., its tidal radius; Clusters with larger $r_{\rm t}$ and smaller c have smoother drop in their ACFs. In the examples shown in Figure A1 all clusters have the same $r_{\rm t}$, and thus the steepness of the drop of their ACF depends only on their concentration parameter.

A2.2 EFF-Profile Clusters

The outskirts of young stellar clusters, located in star-forming regions of the Magellanic Clouds, demonstrate extended outer envelopes, which cannot be represented by King's semi-empirical model (e.g., King 1962), designed for tidally truncated globular clusters. Elson, Fall & Freeman (1987) developed an empirical model more suitable to describe the stellar surface density profile of such clusters (from hereon the EFF model). We base our simulations of centrally-concentrated clusters on this model.

The surface stellar density of the cluster according to the EFF model is described as:

$$f(r) \;=\; f_0 \left[1 + \left(\frac{r}{\alpha}\right)^2\right]^{-\gamma/2} + f_{\rm field}, \qquad \text{(A2)}$$

where f_0 is the central stellar surface density, α is a measure of the core radius and γ is the power-law slope which describes the decrease of surface density of the cluster at large radii; $f(r) \propto r^{-\gamma/2}$ for $r \gg a$. The uniform background density is given by $f_{\rm field}$. For comparison, a King profile (Eq. A1) for $r_{\rm t} \gg r_{\rm c}$ would be described as:

$$f(r) \;=\; f_0 \left[1 + \left(\frac{r}{r_{\rm c}}\right)^2\right]^{-1} + f_{\rm field}. \qquad \text{(A3)}$$

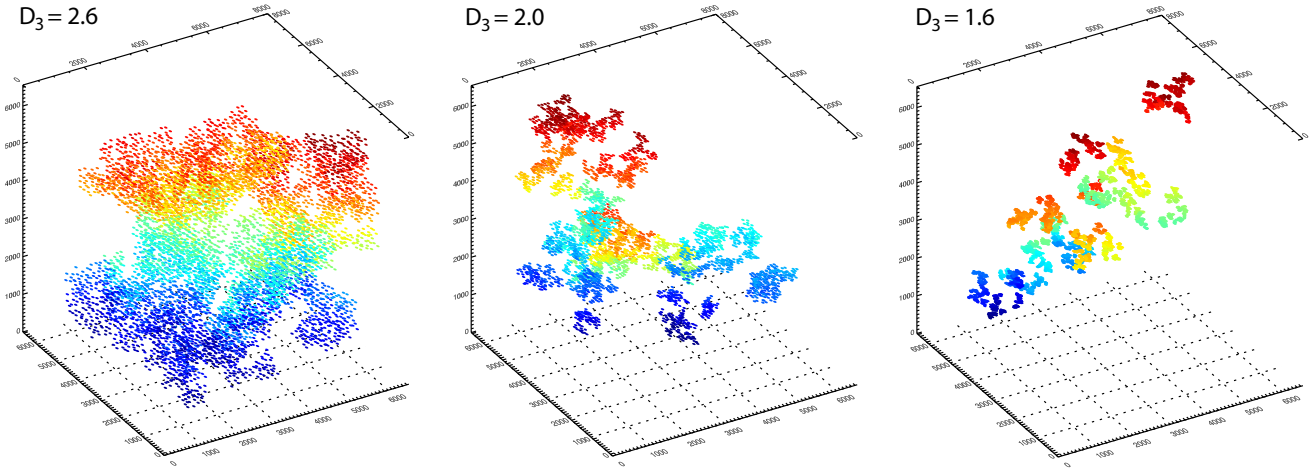

Figure A4. Sample of our simulations of three self-similar stellar distributions. The distributions of few thousand stars with fractal dimensions $D_3 = 1.6, 2.0$ and 2.6 are shown. Note the trend of stellar clustering to higher clumpiness as D_3 becomes smaller, i.e., self-similarity becomes stronger. On the other hand, the fractal dimension of $D_3 = 2.6$ is very close to the geometrical dimension, and thus the corresponding distribution is very close to a random. Points are colored according to their z-axis positions.

The basic parameters of the EFF model, α, γ and $f_{\rm field}$, are measured from the fitting of observed profiles with the function of Eq. (A2).

In order to determine the ACF of clusters following EFF profiles, and compare it to that for NGC 346, we simulate clusters that contain the same number of stars as the observed field of NGC 346 placed in a comparable field-of-view. Apart from the total number of stars of the cluster, we construct our EFF centrally concentrated clusters by providing as input parameters its core radius, $r_{\rm c}$, and the outer surface density index, γ. For reasons of simplicity we ignore the constant contribution of the field, assuming $f_{\rm field} = 0$.

According to the EFF model, the relation of α to the core radius is given from Eq. (A2) assuming no contribution from the field:

$$r_{\rm c} \quad = \quad \alpha(2^{2/\gamma} - 1)^{1/2}. \qquad \text{(A4)}$$

Our simulated clusters have $r_{\rm c}$ and γ values comparable to typical values for young clusters in the Magellanic Clouds (Mackey & Gilmore 2003a,b). In Figure A2 we show the ACFs of five EFF clusters with the same typical value of $\gamma = 3$ and different core radii. Figure A3 demonstrates the constructed ACFs for such clusters keeping the core radius constant at the typical value of $r_{\rm c} = 8''$ while varying the profile index γ within the range of observed values.

Both Figures A2 and A3 demonstrate the dependance of the shape of the ACF of centrally condensed clusters on the assumed structural parameters of the clusters. In Figure A2 can be seen that, for clusters with the same number of stars, larger $r_{\rm c}$ produced more shallow ACFs in particular at smaller separations. The reason for this behavior is that stars would be confined in a narrow area (with short separations) if the core were small. A larger core for the cluster forces them to be distributed over a wider area with higher separations among them, flattening the ACF at small separations. These clusters will appear in the ACF plot 'less clustered' than those which are more centrally concentrated, i.e., in smaller cores. On the other hand, as shown in Figure A3, if the core remains unchanged, the surface density profile slopes change accordingly the decrease of the ACF at large separations. Steeper density profiles lead to ACFs, which are steeper at large separations. The slope of the ACF at smaller separations remains unchanged, while its absolute values are smaller (less clustered) for more shallow stellar surface density profiles at the outskirts of the clusters.

Both figures with the ACFs of EFF-profile clusters show a change in their separations dependence, i.e., a 'breaking' of the ACF slope, at different scales. In Figure A2, the use of clusters with the same γ demonstrates that the radial distance where the separation dependence of ACF changes, i.e., where the power-law 'breaks', depends on how well concentrated the clusters are, i.e., on their $r_{\rm c}$. Therefore, the separation, where the break occurs may be related to a radial scale, which is characteristic for its stability[5].

A3 The Autocorrelation Function of Self-Similar Distributions

In this section we consider the ACF of self-similar, i.e., fractal stellar distributions. We construct three-dimensional artificial fractal distributions with the application of a reverse box-counting algorithm by first defining a cube of side-length 1. Next, this cube is divided into $\mathcal{N}_{\rm div}^3$ equal sub-cubes, of side-length $1/\mathcal{N}_{\rm div}$, which is the first generation of 'children'. $\mathcal{N}_{\rm ran}$ of these sub-cubes are then randomly selected to become parents themselves and further divided into $\mathcal{N}_{\rm div}^3$ child sub-cubes, and the process is repeated recursively, terminating at the desired level of recursion. At this stage each of the smallest (final generation) sub-cubes has a star placed in it. Finally, we normalize the three-dimensional coordinates of these stars to a total side-length of the order of our observed field-of-view[6]. The counting-box fractal dimension depends on both $\mathcal{N}_{\rm div}$ and $\mathcal{N}_{\rm ran}$, and is defined as

$$D \equiv \frac{\ln\left(\mathcal{N}_{\rm ran}\right)}{\ln\left(\mathcal{N}_{\rm div}\right)}. \qquad \text{(A5)}$$

Normally we use $\mathcal{N}_{\rm div} = 2$, in which case there are 8 sub-cubes (children) in every generation. The probability that a child cube will further be divided and become a parent is $\mathcal{N}_{\rm div}^{(D-3)}$. For lower

[5] We explored this dependance for clusters following a King profile in Appendix A2.1.

[6] We assume an average side-length of 6656 pixels, corresponding to $\simeq 5.55'$, or $\simeq 94$ pc.

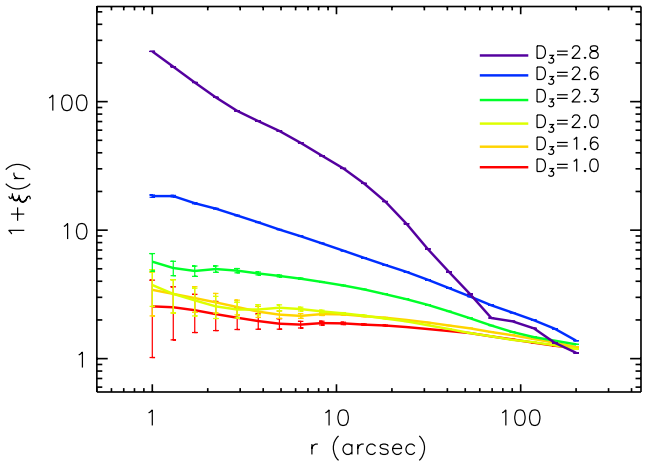

Figure A5. ACFs of six different self-similar stellar distributions, having fractal dimensions of $D_3 = 1, 1.6, 2, 2.3, 2.6$ and 2.8. A sample of one distribution out of several constructed for each D_3 is shown here. These plots show that the ACFs of fractal stellar concentrations should monotonically increase for smaller stellar separations, unlike what we observe in NGC 346.

D, this probability is lower and the distribution becomes more 'porous'. This technique was originally implemented by various authors (see, e.g., Bate et al. 1998; Cartwright & Whitworth 2004).

The produced fractal distributions contain specific stellar numbers by culling randomly the stars that populate the final samples. The number of iterations, i.e., of produced generations, depends on the total number of stars to populate the distribution, $N_\star$ and $\mathcal{N}_{\rm ran}$ as $N_{\rm gen} = \log(N_\star)/\log(\mathcal{N}_{\rm ran})$. Normally we require 10,000 stars to populate our fractal distributions, and thus we produce about 13 generations in each simulation. To avoid an obviously regular structure, we add a bit noise to the positions of the stars, by repositioning every star by a random infinitely small fraction of the sub-cube size. The examples of three such fractal distributions are shown in Figure A4.

The ACFs of indicative self-similar distributions of approximately 5,000 stars with fractal dimensions D_3 between 1.0 and 2.8, are shown in Figure A5. These ACFs show a monotonous decrease with stellar separation, and no indication of a change of slope at a specific scale, unlike what we find in NGC 346. We examined the effect of different viewing angles of the distributions to their two-dimensional projections and the subsequent effect to the produced ACF, and we found that – at least for these stellar numbers of $\sim$5,000 – the derived ACFs show no difference at all, with the corresponding indexes remaining essentially unaffected. It should be noted that the pure 3D fractals generated by the box counting method, after projected on the 2D plane, produce a "wiggle" in their ACF, which nevertheless does not affect their monotonous trend. The scale where this wiggle appears seems to depend on the fractal dimension, occurring for low fractal dimensions at larger scales than for higher fractal dimensions. In the case of the best representative simulations ($D_3 \sim 2.3$) this wiggle occurs at separations $\lesssim 2''$.

APPENDIX B: RELATION BETWEEN THE FRACTAL DIMENSIONS D_3 AND D_2 THROUGH THE ACF INDEX η

The application of the ACF provides a measurement of the two-dimensional fractal dimension D_2 of the considered ensemble through its index η (see, e.g., Section 3). However, we construct

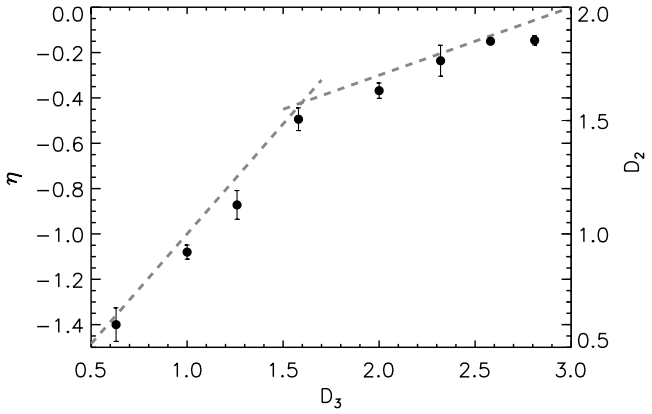

Figure B1. Calibration relation between the three-dimensional fractal dimension D_3, the ACF index η, and the corresponding two-dimensional fractal dimension D_2, derived from our simulated self-similar stellar distributions.

our simulated fractal distributions in a volume, providing as basic input parameter the three-dimensional fractal dimension D_3, and there is no direct relation between D_3 and D_2. A simple conversion $D_3 = D_2 + 1$ is usually cited, which, however, applies only if the perimeter-area dimension of a projected 3D structure is the same as the perimeter-area dimension of a slice (Elmegreen & Scalo 2004). We utilize our simulations of self-similar stellar distributions to provide a more general conversion between D_3 and η, and consequently between D_3 and D_2. This empirical conversion can be very useful for comparing results from methods that measure D_2 to those from methods that provide measurements for D_3 (see, e.g., Federrath et al. 2009, for a discussion on the available methods), with no need for assuming the simple relation $D_3 = D_2 + 1$.

Since in our box-counting simulations we have to use integer numbers for $\mathcal{N}_{\rm ran}$ and $\mathcal{N}_{\rm div}$, there is a limited number of input values for D_3 that can be applied. We performed simulations assuming two numbers for $\mathcal{N}_{\rm div}$ (2 and 3) and established a set of 8 self-similar distributions with different D_3, which span the complete realistic range of values between $D_3 = 0.5$ and $\lesssim 3$. Then we constructed their ACFs and determined the corresponding indexes η, as well as the corresponding two-dimensional fractal dimensions D_2 from the relation $D_2 = 2 + \eta$. The derived empirical calibration is shown in Figure B1. From this figure one can see that D_2 almost equals D_3 only for $D_3 \lesssim 1.6$; this one-to-one relation is represented by the left-hand dashed grey line. For larger values of D_3, the derived D_2 converges toward its maximum possible value of 2 while D_3 approaches its own maximum of 3, having another linear dependence to each other, demonstrated by the right-hand dashed grey line. A simple functional form that can thus represent this relation is:

$$D_2 \simeq \begin{cases} D_3 \ , \ \text{for } D_3 \leqslant 1.6 \\ \\ 1.1 + 0.3\, D_3 \ , \ \text{for } D_3 \geqslant 1.6 \end{cases} \qquad \text{(B1)}$$

It is worth noting that for typical D_3 values derived for turbulent-induced hierarchy, measured in interstellar gas ($D_3 \sim 2.3$), the corresponding D_2 value according to our conversion is $D_2 \sim 1.8$. The errors shown in Figure B1 are the standard deviations of the derived values for η after performing few realizations in the construction of the synthetic fractal distributions for each D_3 value.

REFERENCES

Alfaro, E. J., & Sánchez, N. 2011, Computational Star Formation, 270, 81

Allison, R. J., Goodwin, S. P., Parker, R. J., Portegies Zwart, S. F., & de Grijs, R. 2010, MNRAS, 407, 1098

Arzoumanian, D., André, P., Didelon, P., et al. 2011, A&A, 529, L6

Bastian, N., Gieles, M., Ercolano, B., & Gutermuth, R. 2009, MNRAS, 392, 868

Bate, M. R., Clarke, C. J., & McCaughrean, M. J. 1998, MNRAS, 297, 1163

Baumgardt, H., & Kroupa, P. 2007, MNRAS, 380, 1589

Binney, J., & Tremaine, S. 1987, Galactic Dynamics, Princeton University Press, Princeton, NJ

Bonnell, I. A., Smith, R. J., Clark, P. C., & Bate, M. R. 2011, MNRAS, 410, 2339

Bonnell, I. A., Bate, M. R., & Vine, S. G. 2003, MNRAS, 343, 413

Cartwright, A., & Whitworth, A. P. 2004, MNRAS, 348, 589

Cartwright, A., & Whitworth, A. P. 2009, MNRAS, 392, 341

Cignoni, M., Tosi, M., Sabbi, E., Nota, A., & Gallagher, J. S. 2011, AJ, 141, 31

Clark, P. C., Klessen, R. S., & Bonnell, I. A. 2007, MNRAS, 379, 57

Da Rio, N., Gouliermis, D. A., & Gennaro, M. 2010, ApJ, 723, 166

Dale, J. E., Ercolano, B., & Bonnell, I. A. 2013, MNRAS, 430, 234

Dolphin, A. E. 2000, PASP, 112, 1383

Efremov, Y. N., & Elmegreen, B. G. 1998, MNRAS, 299, 588

Efremov, Y. N. 2009, Astronomy Letters, 35, 507

Elmegreen, B. G. 2011, EAS Publications Series, 51, 31

Elmegreen, B. G. & Falgarone, E. 1996, ApJ, 471, 816

Elmegreen, B. G. & Elmegreen, D. M. 2001, AJ, 121, 1507

Elmegreen, B. G., & Scalo, J. 2004, ARA&A, 42, 211

Elmegreen, B. G., Elmegreen, D. M., Chandar, R., Whitmore, B., & Regan, M. 2006, ApJ, 644, 879

Elson, R. A. W., Fall, S. M., & Freeman, K. C. 1987, ApJ, 323, 54

Falgarone, E., Phillips, T. G., & Walker, C. K. 1991, ApJ, 378, 186

Federrath, C., Klessen, R. S., & Schmidt, W. 2009, ApJ, 692, 364

Feigelson, E. D., Getman, K. V., Townsley, L. K., et al. 2011, ApJS, 194, 9

Gieles, M., & Portegies Zwart, S. F. 2011, MNRAS, 410, L6

Girichidis, P., Federrath, C., Allison, R., Banerjee, R., & Klessen, R. S. 2012, MNRAS, 420, 3264

Gomez, M., Hartmann, L., Kenyon, S. J., & Hewett, R. 1993, AJ, 105, 1927

Goodwin, S. P., & Whitworth, A. P. 2004, A&A, 413, 929

Gouliermis, D. A. 2012, Space Sci. Rev., 169, 1

Gouliermis, D. A., Dolphin, A. E., Brandner, W., & Henning, T. 2006, ApJS, 166, 549

Gouliermis, D. A., Chu, Y.-H., Henning, T., et al. 2008, ApJ, 688, 1050

Harris, W. E. 1996, AJ, 112, 1487

Hénault-Brunet, V., Evans, C. J., Sana, H., et al. 2012, A&A, 546, A73

Henize, K. G. 1956, ApJS, 2, 315

Jeffries, R. D. 2012, Star Clusters in the Era of Large Surveys, Astrophysics and Space Science Proceedings, 163

Karampelas, A., Dapergolas, A., Kontizas, E., et al. 2009, A&A, 497, 703

Kim, S., Staveley-Smith, L., Dopita, M. A., et al. 2003, ApJS, 148, 473

King, I. 1962, AJ, 67, 471

Klessen, R. S., & Burkert, A. 2000, ApJS, 128, 287

Klessen, R. S., & Kroupa, P. 2001, A&A, 372, 105

Kroupa, P. 2004, New Astron. Rev., 48, 47

Kroupa, P. 2008, The Cambridge N-Body Lectures, 760, 181

Krumholz, M. R., & Tan, J. C. 2007, ApJ, 654, 304

Lada, C. J., & Lada, E. A. 2003, ARA&A, 41, 57

Larson, R. B. 1995, MNRAS, 272, 213

Levenberg, K. 1944, Q. Appl. Math., 2, 164

Mac Low, M.-M., & Klessen, R. S. 2004, Reviews of Modern Physics, 76, 125

Mackey, A. D., & Gilmore, G. F. 2003a, MNRAS, 338, 85

Mackey, A. D., & Gilmore, G. F. 2003b, MNRAS, 338, 120

Mandelbrot, B. B. 1983, The fractal geometry of nature (Freeman, San Francisco)

Markwardt, C. B. 2009, Astronomical Data Analysis Software and Systems XVIII, 411, 251

Marquardt, D. 1963, SIAM J. Appl. Math., 11, 431

Megeath, S. T., Gutermuth, R., Muzerolle, J., et al. 2012, AJ, 144, 192

Odekon, M. C. 2006, AJ, 132, 1834

Ossenkopf, V., Krips, M., & Stutzki, J. 2008, A&A, 485, 917

Parker, R. J., Wright, N. J., Goodwin, S. P., & Meyer, M. R. 2013, MNRAS Accepted (arXiv:1311.3639)

Peebles, P. J. E. 1980, The large-scale structure of the universe (Research supported by the National Science Foundation. Princeton, N.J., Princeton University Press, 1980. 435 p.)

Preibisch, T. 2012, Research in Astronomy and Astrophysics, 12, 1

Rubio, M., Contursi, A., Lequeux, J., et al. 2000, A&A, 359, 1139

Sabbi, E., Sirianni, M., Nota, A., et al. 2007, AJ, 133, 44 (Erratum: 2007, AJ, 133, 2430)

Sabbi, E., Sirianni, M., Nota, A., et al. 2008, AJ, 135, 173

Sana, H., de Koter, A., de Mink, S. E., et al. 2013, A&A, 550, A107

Scally, A., & Clarke, C. 2002, MNRAS, 334, 156

Schmeja, S., Kumar, M. S. N., & Ferreira, B. 2008, MNRAS, 389, 1209

Schmeja, S., Gouliermis, D. A., & Klessen, R. S. 2009, ApJ, 694, 367

Spitzer, L. 1987, Dynamical Evolution of Globular Clusters, Princeton University Press, Princeton, NJ

Sreenivasan, K. R. 1991, Annual Review of Fluid Mechanics, 23, 539

Silverman, B. W. 1992, *Density Estimation*, London:Chapman & Hall

Simon, M. 1997, ApJL, 482, L81

Stutzki J., Bensch F., Heithausen A., Ossenkopf V., & Zielinsky M. 1998, A&A336, 697

Scheepmaker, R. A., Lamers, H. J. G. L. M., Anders, P., & Larsen, S. S. 2009, A&A, 494, 81

Westpfahl, D. J., Coleman, P. H., Alexander, J., & Tongue, T. 1999, AJ, 117, 868

Zhang, Q., Fall, S. M., & Whitmore, B. C. 2001, ApJ, 561, 727